V. Discussion

In Fig. 5, the solid line shows the estimated relative error when the above procedure is used for the Frobenius norm and the absolute error is estimated with a 5-point backward average. The deep spike at step 7 is entirely eliminated and approximately from step 40, the exponentially decreasing true error is closely followed by the estimate. Before step 40, there is still a considerable inaccuracy. Here, both the numerator (3) and the denominator (5) contribute to the error; the numerator because the assumption of exponential decrease is not yet justified, the denominator because the Frobenius norm has not yet converged. However, the estimated relative error stays well above 10% during this phase, so a premature stop is avoided.

VI. Conclusion

The accuracy of the ACA convergence criterion when applied to integral equation problems with oscillatory kernels is addressed. Two independent causes of the inaccuracy observed with the original convergence criterion are identified and remedies are proposed which, at a small price in terms of computational speed (20% in the presented example), yield a far more accurate criterion and superior protection against premature truncation of the ACA decomposition.

References

[1] M. Bebendorf, "Approximation of boundary element matrices," *Numer. Matematik*, vol. 86, no. 4, pp. 565–589, 2000.

[2] K. Zhao, M. N. Vouvakis, and J.-F. Lee, "The adaptive cross approximation algorithm for accelerated method of moments computations of EMC problems," *IEEE Trans. Electromag. Compat.*, vol. 47, no. 4, pp. 763–773, Nov. 2005.

[3] G. Hislop, S. Hay, and A. Hellicar, "Efficient sampling of electromagnetic fields via the adaptive cross approximation," *IEEE Trans. Antennas Propag.*, vol. 55, no. 12, pp. 3721–3725, Dec. 2007.

[4] R. Maaskant, R. Mittra, and A. Tijhuis, "Fast analysis of large antenna arrays using the characteristic basis function method and the adaptive cross approximation algorithm," *IEEE Trans. Antennas Propag.*, vol. 56, no. 11, pp. 3440–3451, Nov. 2008.

[5] A. Heldring, J. M. Tamayo, E. Ubeda, and J. M. Rius, "Accelerated direct solution of the method-of-moments linear system," *Proc. IEEE*, vol. 101, no. 2, pp. 364–371, Feb. 2013.

[6] M. Bebendorf and S. Rjasanow, "Adaptive low-rank approximation of collocation matrices," *Computing*, vol. 70, pp. 1–24, Mar. 2003.

[7] J. Laviada, R. Mittra, M. R. Pino, and F. Las-Heras, "On the convergence of the ACA," *Microwave Opt. Technol. Lett*, vol. 51, no. 10, pp. 2458–2460, Oct. 2009.

[8] A. Heldring, J. M. Rius, J. M. Tamayo, J. Parrón, and E. Ubeda, "Multiscale compressed block decomposition for fast direct solution of method of moments linear system," *IEEE Trans. Antennas Propag.*, vol. 59, no. 2, pp. 526–536, Feb. 2011.

[9] G. Golub and C. F. Van Loan, *Matrix Computations*, 4th ed. Baltimore, MD, USA: Johns Hopkins Univ. Press, 2013.

[10] M. W. Berry, S. A. Pulatova, and G. W. Stewart, "Algorithm 844: Computing sparse reduced rank approximations," *ACM Trans. Math. Software*, vol. 31, no. 2, pp. 252–269, Jun. 2005.

A Frequency Reconfigurable Transmitter Antenna With Autonomous Switching Capabilities

Lee Hinsz and Benjamin D. Braaten

***Abstract*—Frequency reconfigurable antennas have many benefits that can be used to improve the performance of wireless systems. Then again, many existing multiband systems cannot use a frequency reconfigurable antenna because of the additional control signals required to operate the antenna. In this communication, an autonomous frequency reconfigurable antenna topology that does not require these control signals from the radio is presented. To control the antenna, a power splitter and bandpass filter is used to pass a portion of the RF power driving the antenna in a particular band to voltage-doubling circuitry. This voltage-doubler circuit is then used to convert the RF signal into a DC output control voltage which then in turn controls the reconfigurable features of the antenna. By setting the bandpass filter to one of the reconfigurable frequencies, RF power can then be used to reconfigure the antenna in a specific band while not reconfiguring in other bands. This flexibility makes this design very useful for existing and future cost effective wireless systems.**

***Index Terms*—Microstrip antennas and power harvesting, reconfigurable antennas.**

I. Introduction

Multiradio wireless platforms such as mobile internet devices, laptops, smart phones and sensor systems are currently being developed to access many different wireless services such as WiFi, WiMax, 3G, Bluetooth, GPS and UWB over various frequency bands [1]. For these devices to access the spectrum, multiband antennas (i.e., dual-, triple- or quad-band antennas) that require sophisticated filtering are being used. In many cases this filtering may not be cost effective. To reduce filtering requirements, frequency reconfigurable antennas with multiband capabilities and greater complexity can be used. Fortunately, researchers have reduced the complexity and overcome many of the limitations of frequency reconfigurable antennas by embedding novel RF circuitry into the design of a frequency reconfigurable antenna. The designs reported in [2] use software-defined radios to control frequency reconfigurable antennas with PIN diodes. High-efficient MEMS based designs have been reported in [3] to reconfigure several different antenna designs. Other methods such as stepper motors [4], optical cables [5] and fluidic micro-pumps [6] have also been researched and presented as other methods to control frequency reconfigurable antennas. Many of the aforementioned switching techniques improve on the design of reconfigurable antennas; however, each design requires a separate control signal to change the state (i.e., frequency) of the antenna.

The objective of this work is to present a frequency reconfigurable antenna that does not require a separate control signal (i.e., an autonomously controlled frequency reconfigurable antenna). It will be shown that simple RF circuitry can be used to create a new antenna topology which can then be used to bring the existing benefits of reconfigurable antennas to wireless systems and additionally not require a separate control signal. Improvements to existing multiband wireless

Manuscript received August 29, 2013; revised October 31, 2013; accepted March 26, 2014. Date of publication April 08, 2014; date of current version July 02, 2014.

The authors are with the Department of Electrical and Computer Engineering, North Dakota State University, Fargo, ND 58102 USA (e-mail: benbraaten@ieee.org).

Color versions of one or more of the figures in this communication are available online at http://ieeexplore.ieee.org.

Digital Object Identifier 10.1109/TAP.2014.2316298

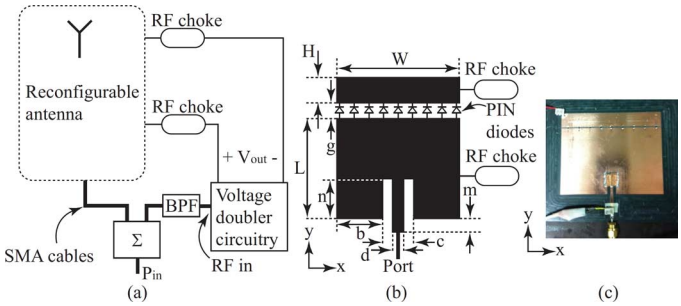

Fig. 1. (a) Layout of the autonomous reconfigurable antenna for the use as a transmitter, (b) layout of the prototype reconfigurable patch antenna and (c) the manufactured reconfigurable microstrip patch antenna ($\mathrm{b} = 41.9$ mm, $\mathrm{c} = 7.77$ mm, $\mathrm{d} = 2.40$ mm, $\mathrm{g} = 1.0$ mm, $\mathrm{m} = 25.53$ mm, $\mathrm{n} = 7.0$ mm, $\mathrm{H} = 13.55$ mm, $\mathrm{L} = 62.88$ mm and $\mathrm{W} = 91.21$ mm).

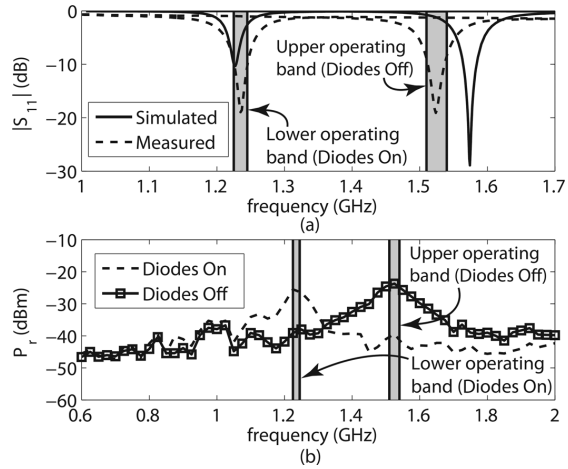

Fig. 2. (a) Simulated and measured S-parameters of the reconfigurable patch antenna only and (b) measured receive power of the reconfigurable patch antenna only at a distance of 2.0 m with the diodes being biased by a DC voltage supply.

systems could include 1) replacing numerous multiband antennas in multistandard-radio base stations with a single autonomous reconfigurable antenna; 2) replacing two orthogonal Yagi antennas and cables with a single reconfigurable antenna with polarization switching capabilities and a single cable and 3) replacing UWB antennas that are being used with multiband frequency-hopping radios with higher gain reconfigurable antennas that do not require a separate control signal.

II. Topology of the Autonomous Reconfigurable Antenna

An illustration of the proposed antenna configuration is shown in Fig. 1(a). The antenna design consists of an arbitrary power divider, bandpass filter, voltage-doubling circuitry and a reconfigurable antenna controlled with voltage V_{out}. The antenna operates in the transmit mode in the following manner: RF power used to drive the antenna is provided to the summing junction of the power divider. Because of the arbitrary power division [7] at this node, a portion of the power is sent to the reconfigurable antenna and the bandpass filter. If the signal is in the pass-band of the filter, RF power is provided to the voltage-doubling circuit and converted to a positive DC voltage V_{out} proportional to the input RF power. If the RF power is large enough, $V_{out} > 0$ and the antenna is reconfigured. If the RF signal driving the antenna is not in the pass-band, then the filter rejects the signal and very little RF power is delivered to the voltage-doubling circuit. This then results in $V_{out} \approx 0$ and the antenna is not reconfigured. Therefore, V_{out} can be used to control the reconfigurable antenna in Fig. 1(a) in an autonomous manner.

III. Prototyping

A prototype to demonstrate the layout in Fig. 1(a) was designed, manufactured and tested. More specifically, each component of the design was evaluated individually; which included a reconfigurable microstrip antenna with PIN diodes for switching, a Wilkinson power divider [8], a band-pass filter and a voltage-doubling circuit. Then, each of the elements were interconnected and the overall antenna was evaluated.

The following comments should be made about the prototype. The topology in Fig. 1(a) is not limited to designs with PIN diodes. This configuration will also work for other designs that require a separate control voltage to reconfigure (i.e., MEMS-based designs). Furthermore, an arbitrary power divider can be used instead of a Wilkinson power divider. This power divider was chosen for demonstration purposes only.

A. The Reconfigurable Microstrip Patch Antenna

Initially, the reconfigurable microstrip patch antenna in Fig. 1(b) was designed on a 0.7874 mm thick Rogers 5880 RT/duroid [9] substrate ($\varepsilon = 2.2$ and $\tan\delta = 0.0004$) in ADS [10]. The layout consisted of a smaller conducting plane that was connected to a larger conducting plane with surface-mount voltage controlled PIN diodes and the control voltage was placed on the conducting planes with RF chokes. The PIN diodes were manufactured by Skyworks [11] (part number: SMP1322) and the RF chokes were manufactured by Mini-circuits (part number: ADCH-80A) [12]. When the diodes are not biased (i.e., turned off), the patch is the smallest and resonates at the upper operating frequency. When the diodes are biased (i.e., turned on), the patch is much larger and the antenna operates at the lower frequency. The manufactured prototype is shown in Fig. 1(c). To represent the biased diodes in ADS, a 1 mm wide printed conductor was used at the location of the diode to connect the two conducting planes. Then, when the diodes were unbiased, the 1 mm wide conductor was removed in ADS to disconnect the two planes.

The S-parameter simulation and measurements are shown in Fig. 2(a) for $N = 9$ diodes. The simulated lower and upper -10 dB bands were 1.22 GHz to 1.23 GHz and 1.54 GHz to 1.60 GHz, respectively, and the measured lower and upper -10 dB bands were 1.22 GHz to 1.245 GHz and 1.56 GHz to 1.58 GHz, respectively. The results agree very well at the lower operating band; however, the upper center frequency was simulated to be 1.574 GHz and measured to be 1.526 GHz. Because the prototypes are being used to demonstrate the proposed design in Fig. 1(a), the measured -10 dB operating bands will be used. These bands are highlighted in grey in Fig. 2 and throughout the communication.

The effects of the PIN diodes on the behavior of the reconfigurable patch were investigated next using the software ADS. In particular, the gain and S_{11} values of the antenna were computed for $N = 1, 3, 5, \ldots, 13$ diodes evenly spaced across the gap. Furthermore, a continuous conductor to provide a uniform contact across the gap for the case where $N \to \infty$ was also simulated for reference. The results from these simulations are presented in Fig. 3 and it is shown that for $N \geq 7$ a good gain and match can be achieved.

Next, the gain of the reconfigurable patch prototype in Fig. 1(c) was measured in an anechoic chamber. This was done by first placing two 1–18 GHz TDK horn antennas (model number: HRN-0118) 2.0 m apart and driving the transmit horn with 14.0 dBm of power with a function generator. The receive power for the field component E_θ was then measured with an Agilent E4402B 3.0 GHz Spectrum Analyzer [13] at the receive horn in both operating bands. Low-loss 26.5 GHz Micro-coax [14] SMA cables 4.5 m in length (part number: UFA210A-0-1800)

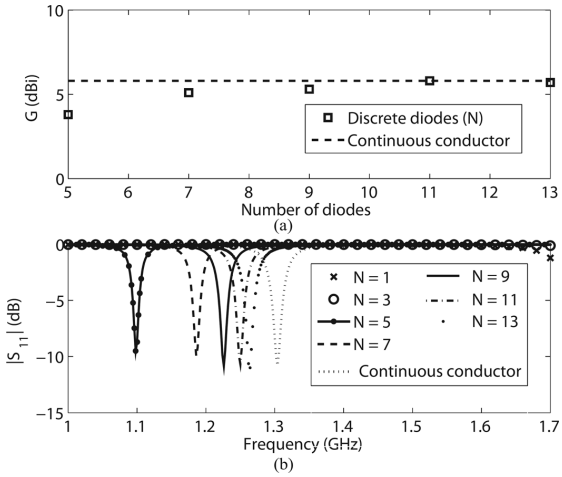

Fig. 3. Simulated (a) gain at resonance and (b) S_{11} of the reconfigurable patch antenna only as the number of diodes are increased.

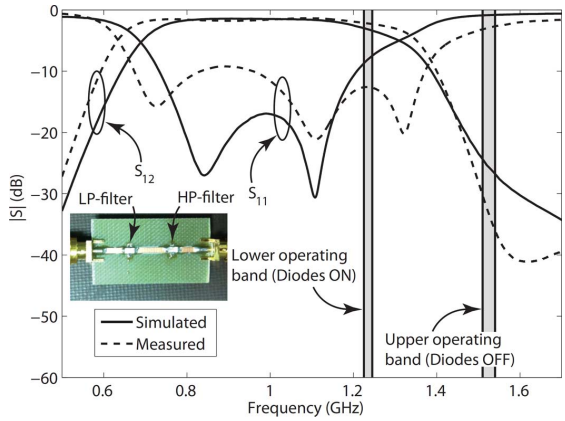

Fig. 4. Simulated and measured S-parameters of the band-pass filter.

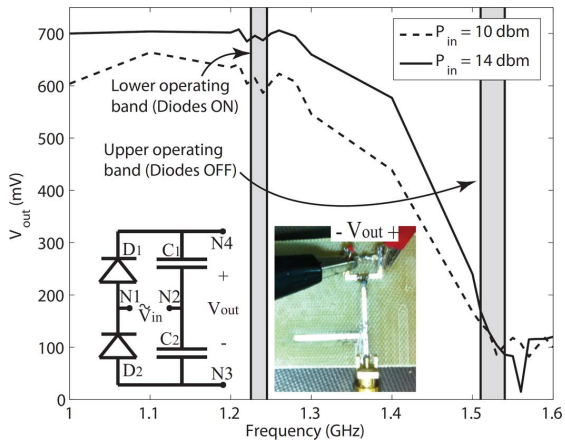

Fig. 5. Measured output voltage of the voltage-doubler circuit with two input power values.

were used to connect the TDK horn antennas to the function generator and spectrum analyzer. Then, the transmit horn being driven by the function generator was replaced by the reconfigurable patch prototype in Fig. 1(c) and the receive power for the field component E_θ on the receive horn antenna was again measured at (0, 0, 2.0 m) in the anechoic chamber. These measurements are shown in Fig. 2(b). For the lower and upper operating bands, the gain was determined to be 0.5 dBi and 4.9 dBi, respectively. For these measurements an external DC voltage supply was connected to the RF chokes and used to switch the reconfigurable patch between the two frequency bands.

For comparison, the gain of the reconfigurable patch was simulated in ADS. The gain of the antenna in the lower and upper operating bands was computed to be 5.1 dBi and 5.6 dBi, respectively. The difference between the simulated and measured gains determined at the upper band are in part due to the power absorbed by the unbiased diodes (as shown in the S_{11} measurements in Fig. 2(a)) and the PCB material losses. The difference between the simulated and measured gains at the lower band are believed to be due to the higher power absorption of the biased diodes, the PCB material losses and the low substrate thickness. The higher absorption of the diodes and substrate effect can be seen by comparing the measured receive powers in both bands in Fig. 2(b).

B. The Band-Pass Filter

Next, the band-pass filter was designed. For this, two surface-mount low- and high-pass filters manufactured by Mini-circuits [12] (low-pass filter part number: LFCN-1000 and high-pass filter part number: HFCN-740) were connected in series. The low-pass filter had a cut-off frequency of 1275 MHz and the high-pass filter had a cut-off frequency of 780 MHz. The filter was designed on a 0.7874 mm thick FR4 grounded substrate in ADS. An image of the filter is shown in Fig. 4 (inset) along with the measured and simulated S-parameters. It can be seen that the lower operating band is passed and the upper operating band is blocked by the high cut-off frequency of the filter; which was measured to be 1.29 GHz. This then ensures that the higher-frequency band is rejected and the lower frequency band of interest is passed to the voltage-doubling circuitry to reconfigure the antenna.

C. The Voltage-Doubling Circuit

The voltage-doubling circuit and prototype board shown in Fig. 5 (inset) was designed and tested next. The diodes were manufactured by Avago Technologies [15] (part number: HSMS-2822-TR1G) and $C_1 = C_2 = 470$ pF. To test the performance of the circuit, a RF signal from a function generator was connected to the input of the band-pass filter with a 0.6 m low-loss Micro-coax cable and the output of the filter was connected across nodes 1 and 2, denoted as $\widetilde{V}_{in}$ in Fig. 5. A PIN diode was then connected between nodes 3 and 4 and the output control voltage V_{out} was measured. The results from these measurements are shown in Fig. 5 for an input power of 10 dBm and 14 dBm. It can be seen that sufficient voltage is supplied by the voltage-doubling circuitry to bias (turn-on) the PIN diodes at the lower band and the voltage is reduced at the upper band to unbias the diodes.

D. Overall Antenna Performance

For overall demonstration, the power splitter, band-pass filter, voltage-doubling circuit and reconfigurable patch were connected to make the prototype antenna shown in Fig. 6(a). The prototype was then placed in an anechoic chamber (shown in Fig. 6(b)) and the radiated power was measured. The same function generator used to test the performance of the reconfigurable patch was used to drive the prototype antenna using the same 4.5 m Micro-coax cable. A TDK 1–18 GHz horn antenna was then connected to an Agilent E4402B 3.0 GHz Spectrum Analyzer again using the same 4.5 m Micro-coax cable as before and E_θ of the radiated field was measured at (0, 0, 2.0 m).

Initially, to determine that the PIN diodes were being fully biased by the voltage-doubling circuitry in the lower band, the input power was increased from 0 dBm to 16 dBm in steps of 2.0 dBm. The receive power was then measured for each of these input power values and the results are shown in Fig. 7(a) at 1225 MHz. A noticeable increase in

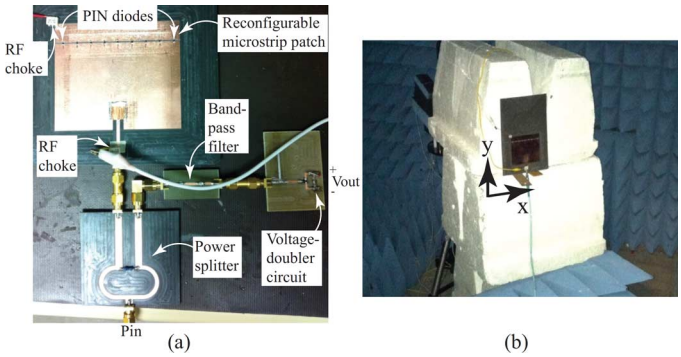

Fig. 6. (a) Picture of the prototype antenna and (b) picture of the prototype antenna being measured in the anechoic chamber (in the x-y plane).

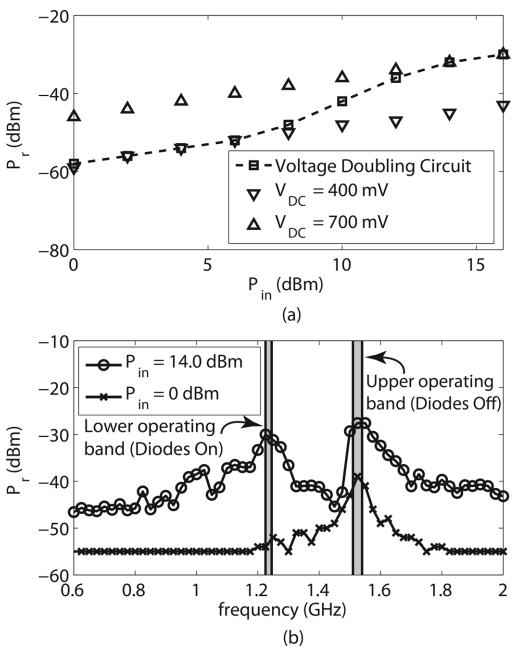

Fig. 7. (a) Comparison of the measured receive power of the prototype antenna when the PIN diodes are biased by the voltage doubling circuitry and a DC voltage supply and (b) measured receive power of the prototype antenna at a distance of 2.0 m with the diodes being biased by the voltage doubling circuitry.

power occurs at 8.0 dBm, indicating that the diodes are beginning to bias. Next, to determine when the diodes were fully biased, the wires connecting the diodes to the voltage doubling circuitry were disconnected and reconnected to a DC voltage supply. The power splitter, band-pass filter and voltage doubling circuitry were left intact in the chamber and the diodes were now being biased by an external voltage supply. Then, the DC voltage was set to 400 mV and 700 mV and the received power was measured in a similar manner. By setting the voltage to 400 mV, the diodes were unbiased and by increasing the voltage to 700 mV, this ensured fully biased PIN diodes and a max radiated field in the lower band. The results from these measurements are shown in Fig. 7(a). When comparing the voltage doubling curve to the receive power values measured for $V_{DC} = 400$ mV and 700 mV, it can be seen that when the input power is at 14.0 dBm, the diodes are being fully biased by the voltage doubling circuitry.

Finally, the diodes were reconnected to the voltage doubling circuitry and the input frequency was swept from 600 MHz to 2.0 GHz. The radiated power was then measured at (0, 0, 2.0 m) and the results from these measurements are shown in Fig. 7(b). Two input powers were used to demonstrate that the diodes were switching on at the lower band. For an input power P_{in} of 0 dBm, radiated power was only observed at the upper operating band which occurs when the diodes are unbiased (as shown in Fig. 7(a)). P_{in} was then raised to 14.0 dBm to provide enough power to bias the PIN diodes (also as shown in Fig. 7(a)).

Next, using the measured received power values, the gains for the lower and upper bands were determined to be -4.0 dBi and 1.0 dBi, respectively. Furthermore, comparing the received power values of the prototype in Fig. 7(b) to the received power values of the reconfigurable patch in Fig. 2(b), a reduction of 4.5 dBm and 3.9 dBm is shown in the lower and upper bands, respectively. These reductions in power are due to the introduction of the power divider and connectors into the measurements, and the additional loss in the lower band is believed to be due to the PIN diodes.

For an analytical comparison, the Friis equation was used next to compute the efficiency of the prototype antenna. Using the measured gains of the reconfigurable patch antenna in the previous section, the expected receive power was computed to be $P_r = -19.3$ dBm and -15.3 dBm in the lower and upper bands, respectively. This then results in a computed power absorption of 3.8 dBm by the power divider, filter and voltage-doubling circuitry in both bands. This compares to the previously measured absorption of 4.5 dBm and 3.9 dBm in the lower and upper bands, respectively.

Finally, the S_{11} values were measured using an Agilent E5071C 100 kHz–8.5 GHz ENA Series Network Analyzer. The output of the network analyzer was set to 10 dBm (max allowable value) and the sweep time was set to 20 sec. This longer sweep time ensured that the voltage doubling circuit was enabled and the diodes were beginning to bias. The results from these measurements gave $|S_{11}| = -14.0$ dB and -19.0 dB in the lower and upper bands, respectively.

IV. Discussion

The prototype in Fig. 6 was meant to demonstrate the antenna topology presented in Fig. 1(a) and many new designs could be developed to improve the performance of the prototype antenna. Further optimization of the design could include an arbitrary power splitter, using switches with less loss, antenna arrays, substrates with lower loss tangents than FR4, thicker substrates for the operating bands chosen in this work, amplifiers to overcome the loss of the circuitry and integration of the entire antenna on a single substrate. Then again, the results in Fig. 7(b) show that the microstrip antenna is autonomously reconfigurable and radiating in the desired bands.

Several applications of the antenna presented in this work were also mentioned earlier. One application could be the replacement of numerous multiband antennas in multistandard-radio base stations with a single autonomous reconfigurable antenna. For comparison, the designs reported in [16]–[19] have gain values that vary from -4 dBi to $+4$ dBi and the geometries range from half to sizes comparable to the antenna design proposed in this communication. The concept of autonomous switching proposed in this communication could be used to replace at least two of these antennas with a single design, save space and have comparable gain values. Furthermore, the concepts could be extended to replacing more than 2 antennas with a single design.

The second application mentioned was related to replacing two orthogonal Yagi antennas and cables with a single reconfigurable antenna and one cable. In some long-distance wireless sensor applications, two coaxial cables are attached to a tower to drive each Yagi antenna. Then, one antenna is used to communicate in one direction with a vertical linear polarization and one antenna is used to communicate in the same direction with a horizontal linear polarization in a different operating band. By using an autonomous polarization reconfigurable antenna instead of two Yagi antennas, a cable and antenna could be completely removed from the tower.

Finally, the third application commented on was the replacement of an UWB antenna. In some applications, the gain of an UWB antenna (such as a spiral) can be as low as -15 dBi below resonance and up to 5 dBi above resonance [20]. However, the entire BW of the spiral antenna may not be needed by a multi-band system and a reconfigurable antenna can be used. Also, a separate control signal may not be available in the existing system that uses a spiral antenna. By implementing the design in this communication, the gain at the desired frequencies could be improved to values above -15 dBi without the requirement of a control signal.

V. Conclusion

An autonomous reconfigurable antenna has been presented and demonstrated. More specifically, the proposed antenna uses RF circuitry to convert a portion of the input power to a DC voltage over a specific operating band. This DC voltage is then used to bias PIN diodes embedded in a reconfigurable antenna. Thus, when the antenna is driven in a specific band, the diodes are biased and when the antenna is driven out of the desired band, the diodes are unbiased. For demonstration purposes, a prototype antenna with RF circuitry and a reconfigurable microstrip antenna was manufactured and tested. Overall, it was shown that the antenna could autonomously switch between two states without the requirement of a control signal. This makes this antenna design very useful for new and existing systems that would benefit from the uses of a reconfigurable antenna.

References

[1] S. Yang, C. Zhang, H. K. Pan, A. E. Fathy, and V. K. Nair, "Frequency-reconfigurable antenna for multiradio wireless platforms," *IEEE Microw. Mag.*, pp. 66–83, Feb. 2009.

[2] H. Song, S.-H. Oh, J. T. Aberle, B. Bakkaloglu, and C. Chakrabarti, "Automatic antenna tuning unit for software-defined and cognitive radio," in *IEEE Antennas Propag. Soc. Int. Symp. Dig.*, Honolulu, HI, USA, Jun. 9–15, 2007, pp. 85–88.

[3] D. E. Anagnostou, Z. Guizhen, M. T. Chryssomallis, J. C. Lyke, G. E. Ponchak, J. Papapolymerou, and C. G. Christodoulou, "Design, fabrication, and measurements of an RF-MEMS-based self-similar reconfigurable antenna," *IEEE Trans. Antennas Propag.*, vol. 54, no. 2, pp. 422–432, Feb. 2006.

[4] Y. Tawk, J. Costantine, K. Avery, and C. G. Christodoulou, "Implementing a cognitive radio front-end using rotatable controlled reconfigurable antennas," *IEEE Trans. Antennas Propag.*, vol. 59, no. 5, pp. 1773–1778, May 2011.

[5] Y. Tawk, J. Costantine, S. Hemmady, G. Balakrishnan, K. Avery, and C. G. Christodoulou, "Demonstration of a cognitive radio front end using an optically pumped reconfigurable antenna system (OPRAS)," *IEEE Trans. Antennas Propag.*, vol. 30, no. 2, pp. 1075–1083, Feb. 2012.

[6] D. Rodrigo, L. Jofre, and B. A. Cetiner, "Circular beam-steering reconfigurable antenna with liquid metal parasitics," *IEEE Trans. Antennas Propag.*, vol. 60, no. 4, pp. 1796–1802, Apr. 2012.

[7] A. M. Abbosh, "Design of ultra-wideband three-way arbitrary power dividers," *IEEE Trans. Microw. Theory Tech.*, vol. 56, no. 1, pp. 194–201, Jan. 2008.

[8] D. M. Pozar, *Microwave Engineering*, 3rd ed. Hoboken, NY, USA: Wiley, 2005, pp. 318–323.

[9] Rogers corporation [Online]. Available: www.rogerscorp.com

[10] Advanced design system (ADS) by Agilent technologies [Online]. Available: www.agilent.com

[11] Skyworks Inc. [Online]. Available: www.skyworksinc.com

[12] Mini-circuits [Online]. Available: www.minicircuits.com

[13] Agilent technologies [Online]. Available: www.agilent.com

[14] Micro-coax [Online]. Available: www.micro-coax.com

[15] Avago technologies [Online]. Available: www.avagotech.com

[16] K.-L. Wong and L.-C. Lee, "Multiband printed monopole slot antenna for WWAN operation in the laptop computer," *IEEE Trans. Antennas Propag.*, vol. 57, no. 2, pp. 324–330, Feb. 2009.

[17] T.-W. Kang and K.-L. Wong, "Internal printed loop/monopole combo antenna for LTE/GSM/UMTS operation in a laptop computer," *Microw. Opt. Tech. Lett.*, vol. 52, no. 7, pp. 1673–1678, Jul. 2010.

[18] L.-C. Chou and K.-L. Wong, "Uni-planar dual-band monopole antenna for 2.4/5 GHz WLAN operation in the laptop computer," *IEEE Trans. Antennas Propag.*, vol. 55, no. 12, pp. 3739–3741, Dec. 2007.

[19] S. Yang, A. E. Fathy, S. M. El-Ghazaly, and V. K. Nair, "Novel reconfigurable multi-band antennas for multi-radio platforms," in *Proc. IEEE Radio and Wireless Symp.*, 2008, pp. 723–726.

[20] *Printed Antennas for Wireless Communications*, R. Waterhouse, Ed. West Sussex, U.K.: Wiley, 2007.

Copper and Transparent-Conductor Reflectarray Elements on Thin-Film Solar Cell Panels

Philippe Dreyer, Monica Morales-Masis, Sylvain Nicolay, Christophe Ballif, and Julien Perruisseau-Carrier

This work is dedicated to the memory of Professor Julien Perruisseau-Carrier, of the Ecole Polytechnique Fédérale de Lausanne, Switzerland, who passed away unexpectedly while this paper was being prepared for publication.

***Abstract*—This work addresses the task of integrating reflectarray antennas on thin-film solar cell panels, as a means to save real estate, weight or cost of platforms, such as satellites or transportable autonomous antenna systems. Reflectarray unit cell families, having large phase range, high optical transparency and low microwave loss, are designed to preserve their efficiency in terms of solar cell and reflectarray antenna efficiency. Because there is a trade-off between the optical transparency and microwave surface conductivity of a conductor, both standard copper and transparent conductors were considered here. The results obtained at the unit cell level demonstrate, for the first time, the feasibility of integrating reflectarray on a thin-film solar cell, preserving good performance in terms of both solar cell and reflectarray efficiency. For instance, using copper, measurement at X-band demonstrates a phase range larger than 270° with an average microwave loss of 0.25 dB and average optical transparency in the visible spectrum of 85%. Using transparent conductor contributes to better average transparency (90%) at the cost of increase in microwave loss (2.45 dB).**

***Index Terms*—Antenna, reflectarray, solar cells, transparent conductors.**

I. Introduction

Recently, there has been a growing interest in the integration of antennas with solar cell (SC) to save on space, weight, visual disturbance or costs [1]–[8]. For instance, in space applications, solar panels and communication systems are the two major contributors to the overall size and weight of the satellites. Combining these two systems can, therefore, help in saving on real estate and cost. In urban areas, wireless communication infrastructure can be integrated into solar panels for architectural aesthetics or costs. Finally, the integration of antennas

Manuscript received October 29, 2013; revised February 28, 2014; accepted March 25, 2014. Date of publication April 10, 2014; date of current version July 02, 2014.

P. Dreyer, M. Morales-Masis, S. Nicolay, and C. Ballif are with the Ecole Polytechnique Fédérale de Lausanne (EPFL) - STI - IEL - GR-JPC, CH-1015 Lausanne, Switzerland (e-mail: philippe.dreyer@gmail.com; monica.moralesmasis@epfl.ch; sylvain.nicolay@epfl.ch; christophe.ballif@epfl.ch).

J. Perruisseau-Carrier, deceased, was with the Ecole Polytechnique Fédérale de Lausanne (EPFL) - STI - IEL - GR-JPC, CH-1015 Lausanne, Switzerland.

Color versions of one or more of the figures in this communication are available online at http://ieeexplore.ieee.org.

Digital Object Identifier 10.1109/TAP.2014.2316539